1-1-2007

Suppression of Rayleigh-Benard Convection with Proportional-Derivative Controller

Marcel C. Remillieux
University of Pennsylvania

Hui Zhao
University of Pennsylvania

Haim H. Bau
University of Pennsylvania, bau@seas.upenn.edu

Reprinted in *Physics of Fluids*, Volume 19, Issue 1, Article 017102, January 2007, 10 pages.
Publisher URL: http://dx.doi.org/10.1063/1.2424490

Suppression of Rayleigh-Bénard convection with proportional-derivative controller

Marcel C. Remillieux, Hui Zhao, and Haim H. Bau[a)]
Department of Mechanical Engineering and Applied Mechanics, University of Pennsylvania, Philadelphia, Pennsylvania 19014-6315

(Received 25 March 2006; accepted 21 November 2006; published online 5 January 2007)

We study theoretically (linear stability) and experimentally the use of proportional and derivative controllers to postpone the transition from the no-motion state to the convective state in a circular cylinder heated from below and cooled from above. The heating is provided with an array of individually controlled actuators whose power is adjusted in proportion to temperatures measured in the cylinder's interior. As the proportional controller's gain increases, so does the critical Rayleigh number for the onset of convection. Relatively large proportional controller gains lead to oscillatory convection. The oscillatory convection can be suppressed with the application of a derivative controller, allowing further increases in the critical Rayleigh number. The experimental observations are compared with theoretical predictions. © *2007 American Institute of Physics*.
[DOI: 10.1063/1.2424490]

I. INTRODUCTION

In many technologically relevant processes, it is desired to modify convective patterns in order to optimize process conditions. Since typical convective systems possess many degrees of freedom and are nonlinear, the control task is not trivial. In order to demonstrate the feasibility of controlling such processes and to study the controller's dynamics, we study a model system: Rayleigh-Bénard (RB) convection in a fluid layer heated from below and cooled from above. The RB problem serves as a paradigm of convective processes that occur, among other places, during crystallization and welding.[1]

A considerable amount of (mostly theoretical) work has been devoted to delaying the onset of RB convection. Early attempts that included the use of "open loop" control by imposing predetermined, time-periodic modulations of the temperature difference across the layer[2,3] provided only marginal stabilization. Moreover, such periodic modulation may lead to a subcritical bifurcation,[4] thereby causing the no-motion state to be only conditionally stable. Theoretical studies on the effect of finite amplitude, nonplanar oscillations on the onset of Rayleigh-Bénard cells were also carried out.[5–7] In a fluid with Prandtl number of 10, the critical Rayleigh number was increased by as much as a factor of 16^7.

A much greater level of stabilization can potentially be achieved through the use of feedback control. Using ideas borrowed from linear and nonlinear control theory, one can alter the bifurcation structure of the convective motion in a thermal convection loop heated from below and cooled from above in theory and experiment.[8–12] Briefly, with the aid of various controllers, it is possible to delay the transition from a no-motion to a motion state, suppress the naturally occurring chaotic advection, stabilize otherwise nonstable periodic orbits embedded in the chaotic attractor, render subcritical bifurcation supercritical, and induce chaos under conditions in which the flow normally would be laminar. The thermal convection loop can be viewed as a low-dimension analog of the RB convection.

Tang and Bau[13–18] and Howle[19–22] demonstrated in theory and experiment that similar control ideas can be extended to systems with a large number of degrees of freedom such as the RB problem of a horizontal fluid layer heated from below and cooled from above. In the RB problem, as long as the Rayleigh number is smaller than a critical value Ra_0, the motionless conduction state is globally stable. Using *ad hoc* proportional controllers, Tang and Bau[17] increased the critical Rayleigh number for the transition from the motionless to the motion state in an upright circular cylinder (aspect ratio 1, silicone oil) by a factor of 1.2 while the maximum theoretically predicted stabilization is a factor of 2. Howle[21] increased the critical Rayleigh number by a factor of 4 in experiments carried out with a slender box with an aspect ratio of 6.2. This larger stabilization achieved by Howle is due to the slenderness of the box that retarded three-dimensional instabilities. Shortis and Hall[23] studied theoretically the use of a combination of linear and nonlinear controllers to prevent the occurrence of subcritical bifurcations in non-Boussinesq fluids.

More recently, Or *et al.*[24] and Or and Speyer[25,26] used synthesis methods such as a linear quadratic Gaussian (LQG or H_2) controller to demonstrate that the system can be stabilized at any desired Rayleigh number. The LQG controller requires full state information. Since such information is not typically available, one has to use a state estimator. The construction of a state estimator is complicated by poorly characterized factors such as imperfections in the experimental apparatus and heat interactions with the environment.

As a more modest objective, in this paper, we improve on the work of Tang and Bau[17] in a number of ways. Tang and Bau[17] used digitally controlled, thermal actuators having

[a)]Author to whom correspondence should be addressed. Electronic mail: bau@seas.upenn.edu

relatively large power steps and were able to increase the critical Rayleigh number for the onset of convection by a factor of ~1.2, which falls short of the theoretical prediction of a factor of 2. In accompanying numerical simulations, Tang and Bau[18] showed that the discrepancy between the experiment and theory might have been caused by relatively large actuators' power steps. In this work, we have refined the actuators and examined the effect of this refinement on the critical Rayleigh number. Furthermore, both in theory and experiment,[17,18] it was previously observed that large controller gains lead to oscillatory convection. In this paper, we examine whether the oscillatory convection can be suppressed with the engagement of a derivative controller.

The paper is organized as follows. Section II presents a linear stability analysis of controlled RB convection in an upright circular cylinder. The critical Rayleigh number for the onset of convection is calculated as a function of proportional and derivative controller gains. Section III describes the experimental apparatus. Section IV examines the convective flow in the absence of a controller and establishes a reference state. Section V describes experimental observations of the effects of the proportional and derivative controllers on the critical Rayleigh number for the onset of convection. Section VI concludes.

II. LINEAR STABILITY ANALYSIS

An upright, vertical cylinder of height H and diameter $2R$ is filled with an incompressible, Boussinesq fluid. The cylinder is heated from below and cooled from the above. The lateral wall is insulated. The fluid motion is described with the dimensionless Boussinesq-Oberbeck equation,[27]

$$\frac{1}{\mathrm{Pr}}\left(\frac{\partial \mathbf{u}}{\partial t}+\mathbf{u}\bullet\nabla\mathbf{u}\right)=-\nabla P+\mathrm{Ra}\,Te_z+\nabla^2\mathbf{u}, \tag{1}$$

the continuity equation,

$$\nabla\cdot\mathbf{u}=0, \tag{2}$$

and the energy equation,

$$\frac{\partial T}{\partial t}+\mathbf{u}\cdot\nabla T=\nabla^2 T. \tag{3}$$

In the above, $\mathbf{u}$ is the velocity vector, T is the temperature, t is time, e_z is a unit vector in the vertical (z) direction, p is the pressure, $\mathrm{Pr}=\nu/\kappa$ is the Prandtl number, $\mathrm{Ra}=g\alpha q_0 H^4/(k\kappa\nu)$ is the Rayleigh number, q_o is the nominal heat flux at the lower boundary (in the absence of control), α is the thermal expansion coefficient, g is the gravitational acceleration, ν is the kinematic viscosity, $\kappa=k/(\rho C_p)$ is the thermal diffusivity, and k, ρ, and C_p are, respectively, the fluid conductivity, density, and specific heat. H is the length scale, H^2/κ is the time scale, κ/H is the velocity scale, $q_o H/k$ is the temperature scale, and $\Gamma=R/H$ is the aspect ratio.

We use the cylindrical coordinates $\{r,\phi,z\}$ with the origin centered at the cylinder's mid-height. The boundary conditions consist of no slip at all boundaries

$$\mathbf{u}\left(r,\phi,\pm\frac{1}{2},t\right)=\mathbf{u}(\Gamma,\phi,z,t)=0, \tag{4}$$

an insulating lateral wall

$$\mathbf{n}\cdot\nabla T(\Gamma,\phi,z,t)=0, \tag{5}$$

a cooled, constant-temperature upper boundary

$$T\left(r,\phi,\frac{1}{2},t\right)=0, \tag{6}$$

and controlled heat flux at the lower boundary

$$\mathbf{n}\cdot\nabla T\left(r,\phi,-\frac{1}{2},t\right)=1+F(r,\phi,T). \tag{7}$$

In the above, the function F is the control law, which will be specified later in the paper.

The no-motion state $\{T_0=0.5-z,\mathbf{u}_0=0\}$ is a solution of Eqs. (1)–(3). Expanding the equations around the no-motion state and retaining only the leading-order terms, we have:

$$\frac{1}{\mathrm{Pr}}\frac{\partial\mathbf{u}}{\partial t}=-\nabla P+\mathrm{Ra}\,\theta e_z+\nabla^2\vec{u}, \tag{8}$$

$$\nabla\cdot\mathbf{u}=0, \tag{9}$$

and

$$\frac{\partial\theta}{\partial t}=\nabla^2\theta+\mathbf{u}\cdot e_z. \tag{10}$$

Equations (8)–(10) are linear and subjected to boundary conditions similar to the ones specified in equations (4)–(7). In the above, $\theta=T-T_0$ is the temperature's deviation from the no-motion, conductive value.

The critical Rayleigh number for the onset of convection is determined by solving the appropriate eigenvalue problem.[1] Tang and Bau[13,16] extended linear stability theory to include a proportional feedback controller of the form $F[r,\phi,\theta_0(r,\phi,t)]=-k_P\theta_0(r,\phi,t)$ and showed that the controller can significantly increase the critical Rayleigh number for the onset of convection. In the above θ_0 denotes the mid-height ($z=0$) temperature deviation from its set (conductive value), and the controller does not alter the no-motion state; i.e., $F(r,\phi,0)=0$.

The magnitude of the critical Rayleigh number for the onset of convection in the presence of a controller depends on both the controller's gain and the Prandtl number. As the proportional controller gain (k_P) increases, so does the critical Rayleigh number.[13,17] At low controller gains, the bifurcation from the no-motion state to the motion state is through a real eigenvalue (the principle of exchange of stability holds). Once k_P exceeds a certain critical value, i.e., $k_{P,C}$, the bifurcation occurs through a pair of imaginary eigenvalues (Hopf bifurcation) to time-dependent, oscillatory convection. This behavior is not surprising. When the controller gain is large, the controller overcompensates and the system tends to exhibit oscillations. The magnitude of $k_{P,C}$ depends on the Prandtl number. As the Prandtl number increases, $k_{P,C}$ decreases. Increases in k_P beyond $k_{P,C}$ lead to a reduction in the critical Rayleigh number.

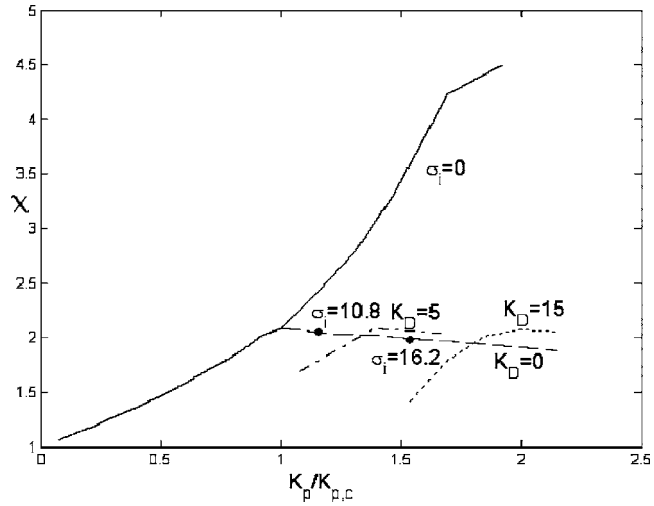

FIG. 1. The normalized, critical Rayleigh number for the onset of convection χ is depicted as a function of the normalized proportional controller gain $k_P/k_{P,C}$. The solid line corresponds to simple bifurcation ($\sigma_I=0$). The heavy dashed line corresponds to Hopf bifurcation into oscillatory convection when $\mathrm{Pr}=10^4$ and the derivative controller gain $k_D=0$. The dashed-dotted and light dashed lines correspond, respectively, to derivative controller gains $k_D=5$ and $k_D=15$.

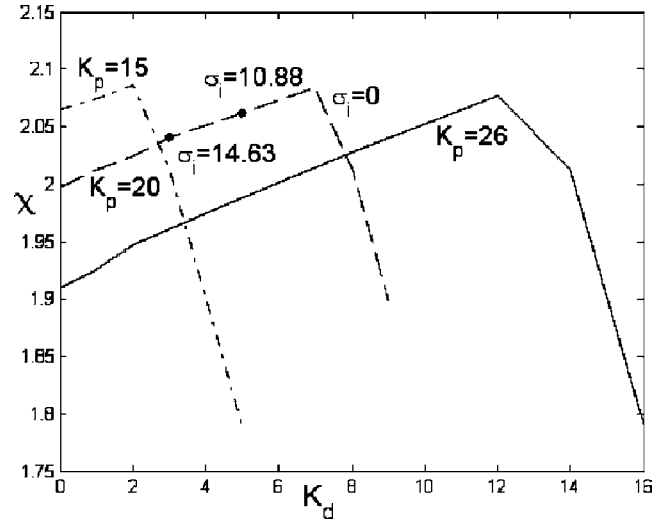

FIG. 2. The normalized critical Rayleigh number χ is depicted as a function of the derivative controller gain k_D when $\mathrm{Pr}=10^4$ and $k_P=15$ (short dashed line), 20 (dashed line), and 26 (solid line).

Often, the transition to oscillatory convection can be delayed with the aid of a derivative feedback controller that damps the oscillations. To accommodate proportional-derivative control, we write the control law:

$$\mathbf{n}\cdot\nabla\theta\left(r,\phi,-\frac{1}{2},t\right)=-k_P\theta(r,\phi,0,t)-k_D\frac{\partial}{\partial t}\theta(r,\phi,0,t), \tag{11}$$

where k_D is the derivative controller's gain.

To compute the critical Rayleigh numbers of the controlled system, we use the multiphysics, finite element program FEMLAB.[28] We project the partial differential equations onto a finite element space and obtain the set of ordinary differential equations:

$$D\frac{dX}{dt}=AX. \tag{12}$$

The above equations include the conservation equations and the boundary conditions. The stability of the system (12) is determined by computing the eigenvalues (σ) of the operator ($D^{-1}A$), where A depends on the Rayleigh number and the controller gains k_P and k_D. Of particular interest is the eigenvalue with the largest real part: $\sigma_1=\sigma_R+I\sigma_I$. At marginal stability, $\sigma_R=0$.

In the absence of a controller ($k_P=k_D=0$) and using 4700 quadratic elements, we computed $\mathrm{Ra}_C\sim 3225$. To assure grid independence, the calculations were repeated with various numbers of elements. For example, when 2600 elements were used, the computed critical Rayleigh number was 0.6% larger.

We define χ as the ratio of the critical Rayleigh number in the presence of the controller $\mathrm{Ra}_C(k_P,k_D)$ and the critical Rayleigh number $\mathrm{Ra}_C(0,0)$ in the absence of a controller; i.e., $\chi=\mathrm{Ra}_C(k_P,k_D)/\mathrm{Ra}_C(0,0)$. Figure 1 depicts χ as a function of the proportional controller gain k_p, normalized with $k_{P,C}$, when $\mathrm{Pr}=10^4$. This very large Prandtl number corresponds to the silicone oil that was used in our experiments. The solid and dashed lines correspond to two different branches of the linear stability curve. The solid line represents a simple bifurcation through a real eigenvalue ($\sigma_R=\sigma_I=0$) and exchange of stability. This solid curve is independent of the Prandtl number and of k_D. The dashed line ($\sigma_I\neq 0$ and $k_D=0$) corresponds to a Hopf bifurcation into oscillatory convection. A few representative values of σ_I are specified along the dashed line. The dashed line represents results for large Prandtl numbers (i.e., $\mathrm{Pr}>100$). The solid and dashed lines intersect at $k_P=13$ and $\chi_{\max}\sim 2.1$. As Pr (<100) decreases, $\chi_{\max}$ increases and the dashed line moves upwards. When $\mathrm{Pr}>100$, in the range $0<k_P<13$, the critical Rayleigh number χ increases as the proportional controller gain increases, and reaches the maximum of $\chi_{\max}\sim 2.1$ at $k_P=13$. Further increases in k_P ($>k_{P,C}$) lead to oscillatory behavior of increasing frequency and a gradual decrease in the critical Rayleigh number. The dashed-dotted and light dashed lines depict the marginal stability when derivative controllers with various gains ($k_D=5$ and $k_D=15$) are engaged. Witness that with appropriate combination of proportional and derivative controller gains, it is possible to somewhat increase the critical Rayleigh number when $k_P>k_{P,C}$. Disappointingly, the derivative controller does not appear to increase $\chi_{\max}$.

The occurrence of oscillatory convection at relatively large proportional controller gains is consistent with experimental observations[17] and numerical simulations[18] and with the experimental work presented later in this paper. The above workers did not examine, however, potential benefits of a derivative controller.

To further investigate the effect of the derivative controller on the stability characteristics of the controlled system, Fig. 2 depicts the normalized, critical Rayleigh number χ as a function of k_D when $\mathrm{Pr}=10\,000$ and various values of k_P:

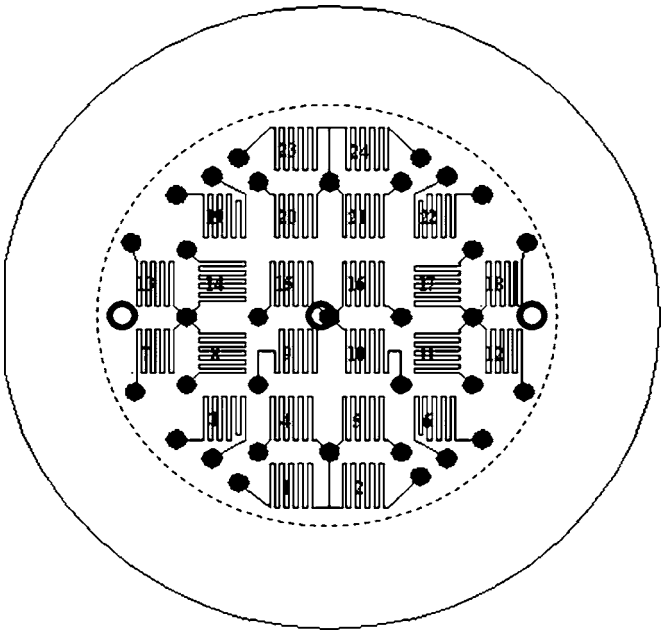

FIG. 3. A schematic depiction of the thermal actuators. The dashed circle represents the inner diameter of the test chamber. The three circles indicate the locations of the three bottom thermocouples.

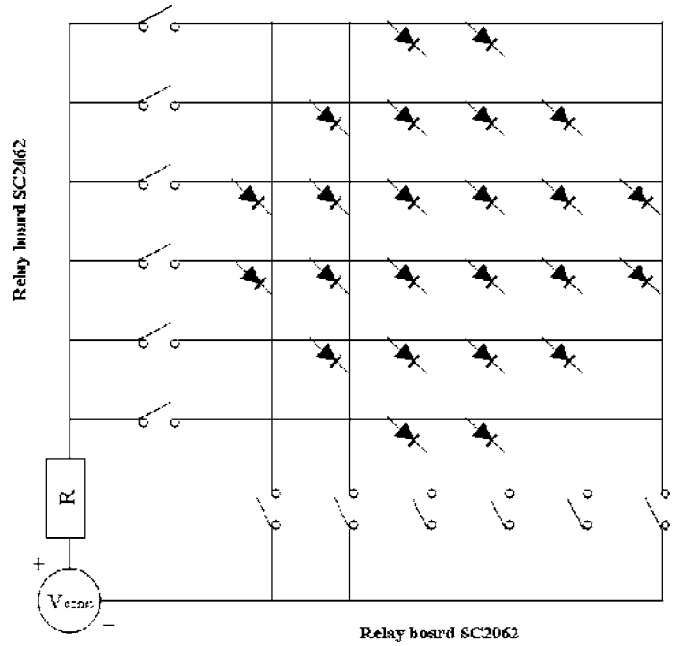

FIG. 4. A schematic depiction of the sensor array used to monitor the temperature at the mid-height of the test chamber

$k_P=15$ (dotted line), $k_P=20$ (dashed line), and $k_P=26$ (solid line). As k_D increases, the critical Rayleigh number χ initially increases, attains a maximum, and then decreases again. Along the ascending part of the curve, the largest eigenvalue is imaginary. Along the descending part of the curve, the imaginary part of the largest eigenvalue is equal to zero (exchange of stability). Like Fig. 1, Fig. 2 indicates that the derivative controller fails to increase $\chi_{\max}$.

We also computed the eigenvectors associated with the largest eigenvalue. In the absence of control, the convective mode consists of a single asymmetric cell. The cylinder can be considered as being divided into two parts by a plane containing the cylinder's axis. The flow is ascending in one half of the cylinder and descending in the other half. In the presence of a controller, the modes have a somewhat more complicated shape. In the interest of space, we do not reproduce here the shapes of the controlled modes. Below, we will compare the theoretical predictions with experimental observations.

III. EXPERIMENTAL SETUP

The test chamber consists of an upright circular cylinder made of 40 mm thick plexiglas with both an inner diameter and height of 35 mm. The chamber was filled with silicone oil (Dow Corning, 1000 cSt). Oil with sufficiently high viscosity was chosen so that the critical Rayleigh number for the onset of convection corresponds to a few degrees Celsius. The lateral wall of the test cell was insulated with a glass fiber sheet, and the upper boundary consisted of a sapphire plate, above which cooling water was continuously circulated to maintain a constant temperature of 25 °C.

A 50.4 mm diameter and 0.5 mm thick silicon wafer formed the bottom boundary (Fig. 3). Using standard microfabrication techniques, we patterned 24 independently controllable, resistance heaters (actuators) on the backside of the silicon wafer. Figure 3 shows the design (AUTOCAD) drawing of the actuating surface. The dashed circle describes the inner diameter of the test chamber. Each heater consisted of a 10 nm thick nichrome, adhesion layer, and a 100 nm thick gold layer. All the heaters shared a common ground and were connected to 24 programmable power amplifiers. The various heaters are labeled with numbers.

The power supplied to the heaters was controlled with 24 digital-to-analog converters (AD558JN, Analog Devices) with 8-bit resolution. The power

$$P_i = \frac{1}{R_i}\left(\frac{n \times V_{\max}}{2^8 - 1}\right)^2 \tag{13}$$

to heater i was adjusted by specifying the integer n ($0<n<255$). In the above, R_i is the resistance of the heater i, and $V_{\max}=5$ V is the maximum voltage available from the programmable power supply. Our earlier numerical simulations[18] indicated that the coarser power steps used in Tang and Bau[17] may have adversely affected the controller's ability to stabilize the system.

In addition to the heaters, three T-type thermocouples (Omega) were soldered to the silicon wafer at the locations indicated with hollow circles (Fig. 3). The temperatures of the actuating surface, the cooling chamber, and the ambient were continuously monitored with in-house calibrated, T-type thermocouples with ±0.2 °C precision.

Twenty-four silicon diodes (MJ 692) located at the cylinder's mid-height monitored the temperatures at various locations across the cylinder's cross section. The diodes were mounted between two sets of six intersecting wires (see Fig. 4 for a schematic). Two relay boards (SC 2062, National Instruments), consisting of six relays each, were connected to

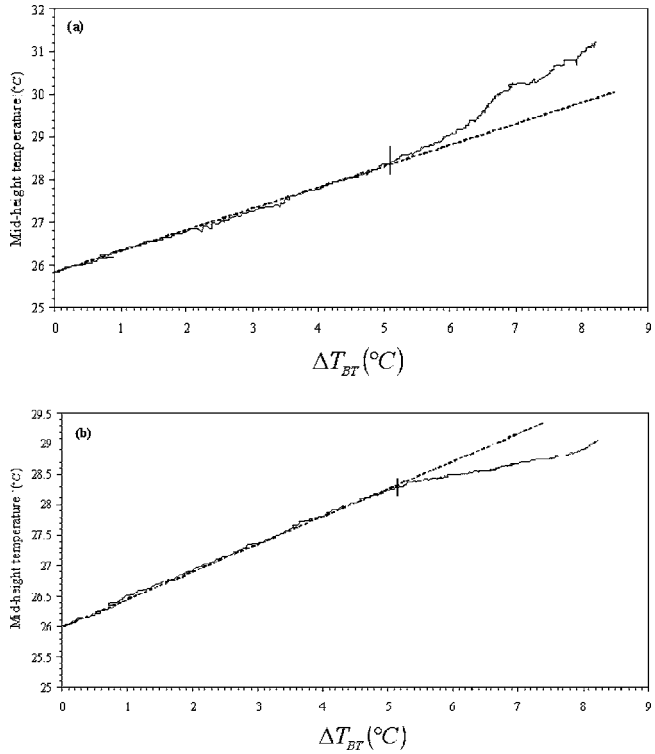

FIG. 5. The mid-height temperature as a function of the average difference between bottom and top temperatures as measured by diode 12 (a) and diode 19 (b).

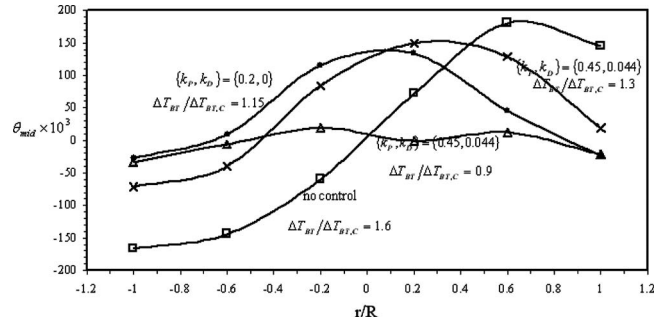

FIG. 6. The normalized mid-height temperature $\theta_{\mathrm{mid}}=(T_i-\bar{T})/\Delta T_{BT}$ as a function of the radial position of the diodes along a diameter where the maximum and minimum θ were observed. The various lines correspond to the uncontrolled case $\{k_P,k_D\}=\{0,0\}$ (□), controlled case $\{k_P,k_D\}=\{0.2\ \mathrm{W/K},0\}$ (•), controlled case $\{k_P,k_D\}=\{0.45\ \mathrm{W/K},0\}$ (×), and controlled case $\{k_P,k_D\}=\{0.45\ \mathrm{W/K},0.044\ \mathrm{J/K}\}$ (△). The average difference between the bottom and top temperatures was about 8.3 °C in all the cases.

the two sets of intersecting wires and were used to address the diodes. A particular diode was selected by closing the corresponding relays on each relay board. All the sensors (thermocouples and diodes) were scanned within approximately 45 s. The thermal diffusion relaxation time of the test cell is $H^2/\kappa \sim 10^4$ s). The scanning time could be reduced at the expense of increased measurement noise. The diode sensors were labeled with numbers. A sensor labeled "*i*" was located directly above the actuator labeled "*i*." When constant current was supplied to the diodes, their voltage varied linearly as a function of their temperature. Thus, the temperature at the diode's location was inferred from the diode's voltage measurement. The diodes were calibrated directly inside the test chamber. After filling the test chamber with silicone oil, eight thermocouples were submerged in the fluid at the level of the diodes. The chamber's temperature was varied, and the diodes' readings were calibrated against the thermocouples' readings. The voltage of each diode was plotted as a function of the average temperature measured by the thermocouples. Linear curves were obtained for all the diodes, with similar slopes but different ordinates at the origin.

IV. CONVECTION IN THE ABSENCE OF CONTROL

Measurements without control were conducted to determine the uncontrolled, reference state. The nominal power was gradually increased from $P_0=0$ to 0.028 W/heater, while the mid-height temperature was continuously measured. Figures 5(a) and 5(b) depict, respectively, the mid-height temperatures recorded by diodes 12 and 19 as functions of the difference between the average bottom temperature and the top temperature ΔT_{BT}. When $\Delta T_{BT} < \Delta T_{BT,C}(0,0) \sim 5.2$ °C, the diodes' temperatures increased linearly as the heating rate and ΔT_{BT} increased. This linear increase signifies predominantly conductive heat transfer. The dashed line is an extrapolation of the straight line. When $\Delta T_{BT} > \Delta T_{BT,C}(0,0)$, the curves deviated from linear behavior. Diode 12 recorded a faster than linear increase in temperature, which suggests that this diode was submerged in ascending flow that brought hot fluid from the cylinder's bottom to the diode's neighborhood. In contrast, diode 19 experienced slower than linear increase in temperature, indicating the presence of descending flow at its location. Figure 5 and other similar records not shown here indicate that the transition from the no-motion to motion states occurred at $\Delta T_{BT}=\Delta T_{BT,C}(0,0) \sim 5.2$ °C.

Figure 6 depicts the normalized mid-height temperature, $\theta_{mid}=(T-\bar{T})/\Delta T_{BT}$, as a function of the radial position of the diodes along the diameter where the maximum and minimum temperatures were observed when the average difference between bottom and top temperature ΔT_{BT} was about 8.3 °C. In the above, $\bar{T}$ denotes the space-averaged, mid-height temperature at a given ΔT_{BT}, and $\Delta T_{BT,C}(k_D,k_P)$ denotes the critical ΔT_{BT} of the controlled system with controller gains k_P and k_D. The lines with the symbols (□), (•), (×), and (△) correspond, respectively, to $\{k_P,k_D\}=\{0,0\}$ (uncontrolled case, $\chi=1.6$), $\{0.2\ \mathrm{W/K},0\}$ (controlled case, $\chi=1.15$), $\{0.45\ \mathrm{W/K},0.044\ \mathrm{J/K}\}$ (controlled case, $\chi=1.3$), and $\{0.45\ \mathrm{W/K},0.044\ \mathrm{J/K}\}$ (controlled case, $\chi=0.9$). In the above, $\chi=\Delta T_{BT}/\Delta T_{BT,C}(k_P,k_D)$ is approximately the ratio between the actual and critical Rayleigh numbers, where the critical temperature difference was determined in the presence of the controller. When $\chi<1$, the temperature distribution (not shown) was nearly uniform with a slight slope next to the side wall, indicating heat interaction with the wall. See Tang and Bau[17] for further details. When $\chi>1$, consistent with theoretical predictions and numerical simulations,[18] in the absence of a controller (□), the cylinder appears to be divided into two halves by a vertical plane containing the cylinder's axis. In one half, the temperatures are above the average, and in the other half, they are below the average.

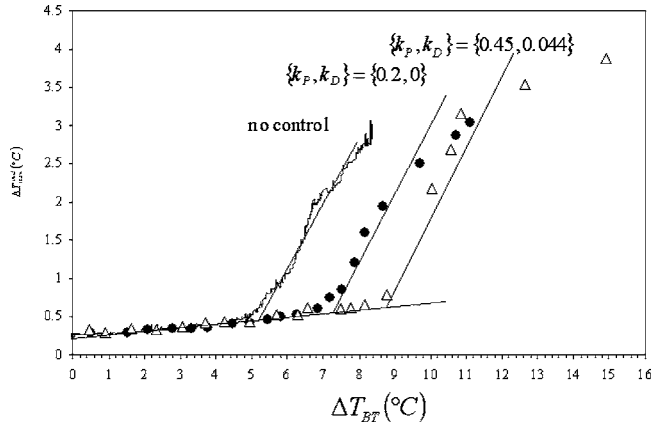

FIG. 7. The maximum mid-height temperature difference as a function of the average difference between the bottom and top temperatures in the uncontrolled case (solid curve), the controlled case $\{k_P,k_D\}=\{0.2\ \mathrm{W/K},0\}$ (•), and the controlled case $\{k_P,k_D\}=\{0.45\ \mathrm{W/K},0.044\ \mathrm{J/K}\}$ (△).

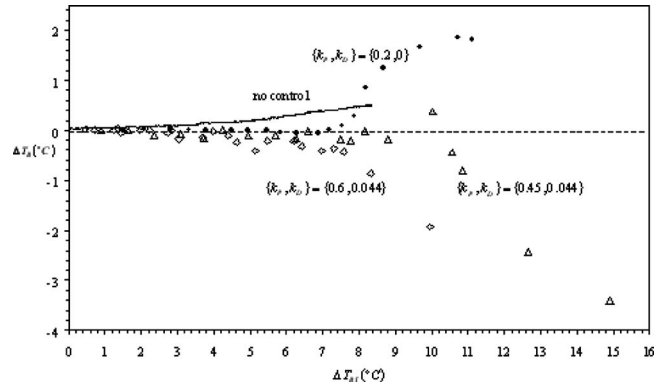

FIG. 8. The bottom temperature difference ΔT_B between the two diagonally opposed thermocouples located at the edges of the heating plate as a function of the average difference between the bottom and top temperatures in the uncontrolled case (solid curve), the controlled case $\{k_P,k_D\}=\{0.2\ \mathrm{W/K},0\}$ (•), the controlled case $\{k_P,k_D\}=\{0.45\ \mathrm{W/K},0.044\ \mathrm{J/K}\}$ (△), and the controlled case $\{k_P,k_D\}=\{0.6\ \mathrm{W/K},0.044\ \mathrm{J/K}\}$ (◇).

This temperature distribution is consistent with a supercritical, single convective cell with fluid ascending in one half of the cylinder and descending in the other half. The temperature profile (□) appears to be slightly slanted next to the lateral wall, indicating some heat losses to the lateral boundary.

Figure 7 depicts the maximum mid-height temperature difference ($\Delta T_{\max}^{\mathrm{mid}}$) as a function of the difference between the average bottom temperature and the top temperatures (ΔT_{BT}) in the absence of control and in the presence of the various controllers described in Fig. 6. Note that when $\Delta T_{BT}=0$ (heaters off), the maximum temperature difference is slightly ($\sim$0.2 °C) above zero. This difference is probably caused by the cooling water's temperature being slightly below the room temperature. In the absence of control and when $\Delta T_{BT}<5$ °C, $\Delta T_{\max}^{\mathrm{mid}}$ increases slowly and nearly linearly as ΔT_{BT} increases. We refer to this regime as subcritical, and we fit the experimental data with a straight line. We surmise that this slight increase is due to weak convection resulting from imperfections in the experimental apparatus. When $\Delta T_{BT}>5$ °C, $\Delta T_{\max}^{\mathrm{mid}}$ increases much more rapidly as the heating rate increases. When $(\Delta T_{BT}-5\ ^\circ\mathrm{C}>0)$ is relatively small, we fitted the experimental curve with a straight line, which we refer to as the supercritical line. The intersection between the sub and supercritical lines occurs at $\Delta T_{BT}=\Delta T_{BT,0}\sim 5.2$ °C and provides an estimate for the bifurcation point. The behavior depicted in Fig. 7 is reminiscent of an imperfect bifurcation.

The critical Rayleigh number $\mathrm{Ra}=g\alpha\Delta T_{BT}H^3/(\kappa\nu)$ that corresponds to $\Delta T_{BT,0}\sim 5.2$ °C is approximately 19 000. We used a temperature-based definition of the Rayleigh number rather than a heat flux-based definition because, due to thermal losses, the portion of the heat flux that actually went into the test cell is not accurately known. The calculation of the Rayleigh number is based on thermophysical property data provided by Dow Corning, the silicone oil manufacturer. The thermal expansion coefficient $\alpha\sim 9.6\times 10^{-4}\ \mathrm{K}^{-1}$, the thermal diffusivity $\kappa\sim 1.08\times 10^{-7}\ \mathrm{m}^2/\mathrm{s}$, and the kinetic viscosity $\upsilon\sim 10^{-3}\ \mathrm{m}^2/\mathrm{s}$. The experimental estimate of the critical Rayleigh number is substantially larger than 3225, the predicted one. This large discrepancy between theory and experiment is due to the presence of the diodes in the test chamber and to the conducting sidewall—neither of which was accounted for in the eigenvalue-based theory of Sec. II. The diodes acted like "baffles," introduced viscous resistance that slowed down the flow, allowed more time for the disturbances to dissipate, and stabilized the flow. We carried out numerical simulations in the appendix to illustrate the significant stabilizing effect of the baffles. Likewise, the presence of the conductive sidewall facilitated dissipation of thermal disturbances and stabilized the flow. We did not account for these effects in Sec. II both because of the geometrical complexity (diodes) involved and because they render the bifurcation imperfect.

Figure 8 depicts the difference between the temperature readings of the two off-center thermocouples ΔT_B (°C) located on the bottom surface as a function of ΔT_{BT} (°C) in the absence of control (solid curve) and in the presence of the various controllers described in Fig. 6. In the purely conductive state, we would expect $\Delta T_B\sim 0$. In the absence of a controller, when $\Delta T_{BT}<\sim 5$ °C, ΔT_B increases slowly as ΔT_{BT} increases. The rate of growth of ΔT_B accelerates when $\Delta T_{BT}>5$ °C. The data is consistent with weak, single cell, subcritical convection when $\Delta T_{BT}<5$ °C.

V. THE RAYLEIGH-BÉNARD CONVECTION WITH FEEDBACK CONTROL

To delay the transition from the motionless state to the motion state to higher Rayleigh numbers, we utilize a proportional-derivative feedback controller. Accordingly, the power supplied to heater (i) is

$$P_i = P_0 - k_p(T_i - T_i^{\mathrm{set}}) - k_d\frac{\partial(T_i - T_i^{\mathrm{set}})}{\partial t}, \tag{14}$$

where P_0 is the nominal power, k_P and k_D are, respectively, the proportional and derivative controller gains, T_i is the temperature read by diode "i," and T_i^{set} is the temperature that diode i would have read in the absence of convection at the specified power P_0.

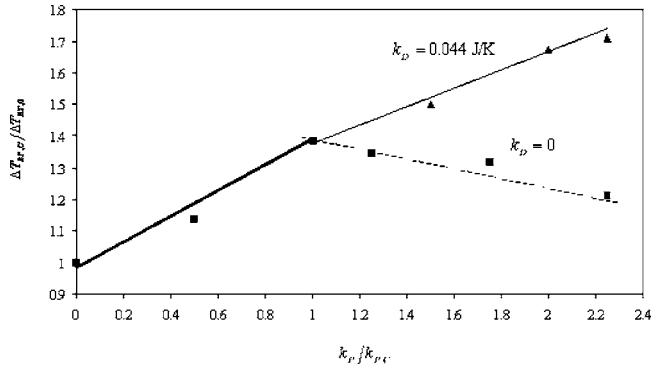

FIG. 9. The average difference between bottom and top temperatures as a function of the normalized controller gain (k_P) when k_D=0 (■) and k_D=0.044 J/K (▲).

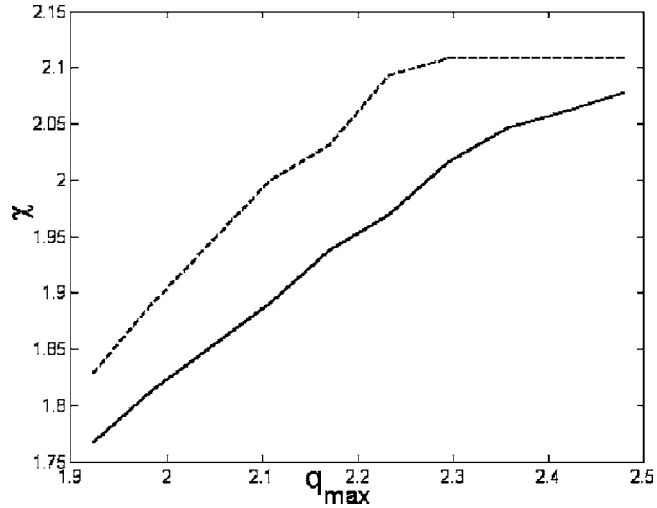

FIG. 10. The critical Rayleigh number as a function of the actuators' maximum power $q_{\max}$ when k_P=13 and k_D=0 (solid line) and when k_P=13 and k_D=2 (dashed line). The initial conditions are $\mathbf{u}$=0 and $T=\lambda(0.5-z)$, where λ=0.9.

In the experiment, we determined the set (desired) temperatures T_i^{set} by taking advantage of the linear dependence of the diodes' temperatures on the power input in the predominantly, conductive regime (see Fig. 5). In the conductive regime, we fit the data with a line of the form:

$$T_i = a_i + b_i P_i. \tag{15}$$

Individual best-fit lines were determined for the 24 diodes with correlation (R-value) better than 0.99. The set temperature was determined by extrapolating these lines to the desired P_i value.

The experimental procedure consisted of turning the controller on, and gradually increasing the power input to the heaters. The diodes' and thermocouples' temperatures were continuously monitored and recorded. After each power increase, a sufficient amount of time was allowed for steady state conditions to be established. Unless otherwise specified, the results presented below are given in terms of the time-averaged steady-state data.

A. Proportional Control

We first consider the case of the proportional controller (k_D=0,k_P>0) that was previously studied by Tang and Bau[17] with cruder power steps. Figure 7 (solid circles) depicts the maximum difference in the mid-height temperature $\Delta T_{\max}^{\text{mid}}$ as a function of ΔT_{BT} (solid circles). Note that the controller delays the transition from the nearly no-motion state to the motion state from $\Delta T_{BT,C}(0.2,0)\sim 5.2$ °C to $\Delta T_{BT,C}(0.2,0)\sim 7.2$ °C. In other words, the proportional controller increased the critical Rayleigh number by about 38% compared to the uncontrolled case. The temperature profile at mid-height (Fig. 6, solid circles) of the supercritical flow (χ=1.15) features a temperature maximum near the cylinder's center.

Figure 8 (solid circles) is consistent with the data reported in Fig. 7. When $\Delta T_{BT}<7.2$ °C, the temperature difference (ΔT_{B}) between the thermocouples located at the bottom of the apparatus is nearly zero. Once $\Delta T_{BT}>7.2$ °C, ΔT_{B} increases as ΔT_{BT} increases.

The proportional controller's effect on the stability of the system is summarized in Fig. 9. The figure depicts the normalized critical temperature difference $\chi=\Delta T_{BT,C}(k_P,0)/\Delta T_{BT,C}(0,0)$ (heavy solid line) for the onset of convection as a function of the normalized proportional controller gain $k_P/k_{P,C}$. The onset of convection was determined using the same method as described in Sec. IV. When $k_P<k_{P,C}\sim 0.2$ W/K, $\Delta T_{BT,C}(k_P,0)$ (solid line) increased as k_P increased, achieving a maximum value of $\sim$7.2 °C at $k_P\sim k_{P,C}$. The proportional controller successfully increased the critical Rayleigh number by nearly a factor of 1.4. Further increases in the proportional controller gain resulted in the saturation of the actuators and oscillatory behavior. In order to maintain the motionless state with proportional controller gains $k_P>k_{P,C}$, it was necessary to reduce the magnitude of the Rayleigh number. In other words, as k_P increased beyond $k_{P,C}$, the critical Rayleigh number decreased (dashed line). Although qualitatively, the behavior depicted in Fig. 9 is similar to the theoretical predictions of Fig. 1, the maximum stabilization $\chi_{\max}\sim 1.4$ obtained in the experiment falls short of the theoretical prediction ($\chi_{\max}$=2.1). We attribute this shortfall to occasional saturation of the actuators, which was observed in the experiments but not accounted for in the linear theory (Sec. II).

To examine the effect of actuator saturation on the controller's performance, we carried out a sequence of numerical experiments in which the actuator's power was restricted $[0<1+F(r,\phi,t)<\text{q}_{\max}]$. In the foregoing expression, the actuator's maximum power is normalized with the critical heat flux for the onset of convection in the controller's absence. Numerical simulations were carried out for various Rayleigh numbers with initial conditions corresponding to no-motion and a perturbed temperature field $T(x,z,0)=\lambda(0.5-z)$. In each case, we computed the kinetic energy of the fluid as a function of time and determined the largest Rayleigh number for which the kinetic energy still decayed to zero. Figure 10 (solid line) depicts the largest normalized Rayleigh number at which a proportional controller successfully stabilized the flow when k_P=13, k_D=0, and λ=0.9. Since the problem is nonlinear, the stability curve depended on the initial condi-

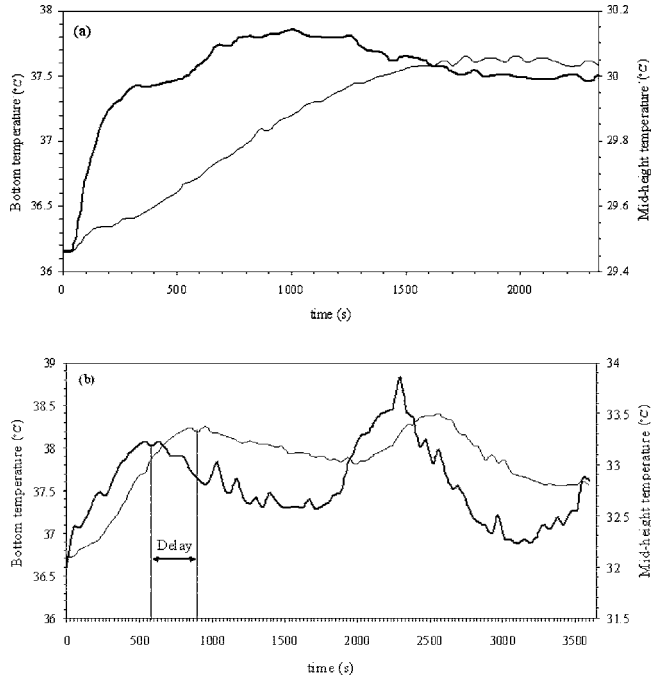

FIG. 11. The average bottom temperature (heavy curve) and the mid-height temperature recorded by diode 19 (light curve) as a function of time following an increase in P_0 from 0.024 to 0.025 W/heater when k_P=0.2 W/K (a) and k_P=0.35 W/K (b).

tions. Witness that as $q_{\max}$ decreases, so does the critical Rayleigh number for the onset of convection. Thus, it is reasonable to attribute the discrepancy between the performance of the controller in theory and experiment to actuator saturations.

The theory predicts that when the Rayleigh number exceeds its critical value when $k_P > k_{P,C}$, time-wise, periodic convection will ensue. This is consistent with our experimental observations. Figures 11(a) and 11(b) depict the temperature of one of the thermocouples located at the bottom of the apparatus (heavy solid line, temperature scale on the left) and the temperature recorded by a diode sensor located at mid-height, at approximately the same radial and azimuthal coordinates as the thermocouple (light solid line, temperature scale on the right), as functions of time when the heaters' nominal power was increased at time $t=0$ from 0.024 to 0.025 W/heater in the presence of the proportional controller. Figures 11(a) and 11(b) correspond, respectively, to controller gains k_P=0.2 W/°C$<k_{P,C}$ and k_P=0.35 W/°C $>k_{P,C}$. In both cases, the step change in the heater's power caused an increase in the bottom's temperature above its nominal value (overshoot) for the new power setting. Following a certain time-delay, the overshoot was felt at the sensor's location. Due to the overshoot in the sensor's temperature, the controller adjusted downwards the heat input to the heater. This mechanism caused oscillations in the heating rate with corresponding oscillations in the sensor's temperature. When the proportional controller's gain was relatively small ($k_P < k_{P,C}$), these oscillations damped out. When the proportional controller gain was large ($k_P > k_{P,C}$), the oscillatory behavior was self-sustained and lasted indefinitely.

In addition to suppressing convection, the controller also modified the supercritical flow patterns. In the absence of a controller, the supercritical flow consisted of a single asymmetric, convective cell. The cylinder could be thought of as divided into two halves by a plane going through its axis. The flow ascended in one half and descended in the other half (Fig. 6, $\{k_P,k_D\}=\{0,0\}$). In the presence of the controllers $\{k_P,k_D\}=\{0.2\text{ W/K},0\}$ and $\{k_P,k_D\}=\{0.45\text{ W/K},0\}$, the maximum temperature occurred near the cylinder's center, indicating a convective pattern with the flow ascending next to the center and descending at the periphery.

B. Derivative Controller

Both the theoretical analysis of Sec. IV and the experiments indicate that increasing the proportional controller gain beyond $k_{P,C}$ leads to decreases in the critical Rayleigh number for the onset of convection. In this section, we investigate the effect of the combined action of the proportional and derivative controllers.

To apply the derivative controller, we need to evaluate the time-derivative dT_i/dt. Due to noise, the temperature's time derivative is subject to fluctuations that may adversely impact the controller's performance. To filter these undesired fluctuations, we constructed a polynomial approximation for the temperature as a function of time:

$$\tilde{T}[i] = \sum_{j=0}^{3} a_j[i]t^j \tag{16}$$

using seven time intervals spaced 45 s apart. In the above, a_j are best-fit coefficients determined by regression. The time derivative was calculated directly from expression (16).

Figure 9 (upright solid triangles and light solid line) depicts $\Delta T_{BT,C}(k_P,k_D)$ as a function of k_P when k_D=0.044 J/K. With the combined action of the proportional and derivative controllers, the Hopf bifurcation into oscillatory convection was suppressed, and the critical temperature difference between bottom and top $\Delta T_{BT,C}(k_P,k_D)$ was increased to about 8.8 °C at k_P=0.45 W/K (see also Figs. 7 and 8, upright, hollow triangles), which represents a 70% increase in the critical Rayleigh number of the uncontrolled system. Experiments were not carried out for larger k_P values since increases in k_P above 0.45 W/K led to frequent saturation of the thermal actuators (heaters).

The nearly uniform, subcritical (χ=0.9), mid-height temperature distribution (Fig. 6, upright, hollow triangles) indicates that the combined proportional-derivative controller has successfully suppressed convection. The supercritical flow in the presence of the proportional-derivative controller (Fig. 6, χ=1.3, symbol "X") appears to consist of ascending flow in the cylinder's interior and descending flow next to the periphery.

In the theoretical analysis (Sec. II), the derivative controller failed to increase $\chi_{\max}$. In contrast, in the experiments, the derivative controller effectively postponed the transition to the motion state. The derivative controller reduced the occurrence of the actuator saturations and hence allowed the proportional controller to be more effective. We mimicked this effect in numerical simulations in which the actuator saturations were accounted for. Figure 10 (dashed line) de-

picts the normalized, critical Rayleigh number for the onset of convection as a function of $q_{\max}$ when $k_P=13$, $k_D=2$, and $\lambda=0.9$. Note that by engaging the derivative controller in addition to the proportional one, we were able to postpone the transition from the no-motion to the motion state to higher Rayleigh numbers than was possible with the proportional controller alone.

VI. CONCLUSIONS

We studied theoretically and experimentally the use of proportional-derivative control to stabilize the no-motion state of a high Prandtl number fluid confined in an upright cylinder with an aspect ratio of 0.5. With the use of a proportional controller alone, the critical Rayleigh number was increased by a factor of 1.4. This is an improvement over prior experiments[17] in which the critical Rayleigh number was increased only by a factor of 1.2. This improvement in performance is attributed to refinements in the thermal actuators. The experiments, however, still fall short of the theoretical prediction that a proportional controller of the type used here can increase the critical Rayleigh number by as much as a factor of 2. The discrepancy between the experiment and theory can be attributed to various idealizations that were made in the theory such as continuously distributed actuators with continuous power variations, no cross-talk (lateral conduction) among the heaters, and, in particular linear actuators (that do not saturate). In contrast, in the experiment, by necessity, we used a finite number of discrete (nonlinear) actuators with discrete variations in the heat input and with limited power output. Numerical simulations, indeed, indicate that when the simulation accounts for actuator saturations, a good qualitative agreement is obtained between theory and experiments.

Both theory and experiment demonstrate the emergence of time-wise oscillatory convection (Hopf bifurcation) once the controller gain has exceeded a certain threshold value. The oscillatory convection can be damped out with the use of a derivative controller. In contrast to the theory, which predicts only marginal stability gains with the engagement of the derivative controller, the proportional-derivative controller in the experiment allowed us to increase the critical Rayleigh number for the onset of convection by as much as a factor of 1.7 (compared to the uncontrolled case). We were not able to increase the critical Rayleigh number even further due to frequent saturation of the thermal actuators at high controller gains.

To achieve additional gains in the critical Rayleigh number, it would probably be necessary to implement a more complex control algorithm that allows all the sensors to interact with all the actuators; i.e., a multiple-input, multiple-output controller. Although linear system theory provides us with powerful tools for the design of such a controller, the implementation in practice is complicated by the differences between the mathematical model and the actual experiment.

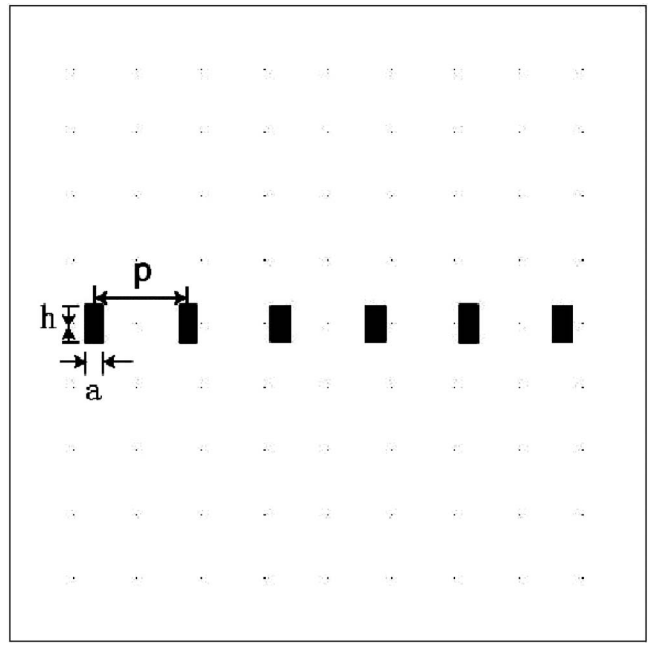

FIG. 12. The domain used in the computations of the effect of baffles on the critical Rayleigh number for the onset of convection.

ACKNOWLEDGMENT

The work was supported, in part, by the National Science Foundation Grant No. CTS-0212998 to the University of Pennsylvania.

APPENDIX: THE EFFECT OF BAFFLES ON RAYLEIGH BÉNARD STABILITY

To examine the diode's effect on the critical Rayleigh number for the onset of convection, we conducted a few numerical simulations. Due to computer memory limitations, we were not able to simulate the three-dimensional, complex geometry with multiple diodes of the experimental apparatus. Instead, we solved an equivalent two-dimensional problem. The two-dimensional geometry corresponds to a cross-section of the apparatus that includes six diodes and a network of lead wires. The cross-sectional area occupied by the baffles in the simulation is equivalent to the cross-sectional area occupied by the diodes.

Figure 12 depicts the computational domain that consists of a two-dimensional square box of height H filled with liquid. The six small boxes of width a and height h uniformly distributed with pitch P and located at the mid-height of the box represent the diodes.

The baffles conduct heat. The temperature distribution inside the baffles satisfies the heat equation

$$\frac{\partial T_s}{\partial t} = \frac{\kappa_s}{\kappa_f}\nabla^2 T_s, \tag{A1}$$

where quantities with subscripts s and f denote, respectively, the properties of the solid baffles and the fluid.

The thermal and hydrodynamic interfacial conditions on the baffles' surfaces are, respectively,

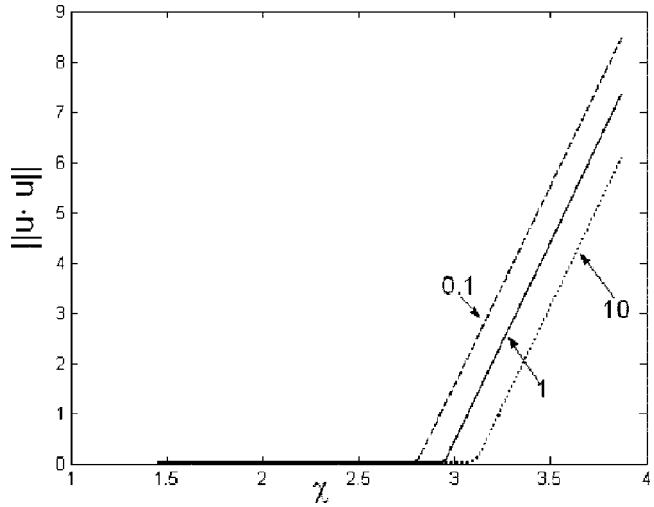

FIG. 13. The kinetic energy $\int \mathbf{u}\cdot\mathbf{u}dA$ as a function of the normalized Rayleigh number. The solid, dotted, and dotted-dashed lines correspond to $\zeta=0.1$, 1, and 10, respectively.

$$T_f = T_s \quad k_s \mathbf{n}\cdot\nabla T = k_f \mathbf{n}\cdot\nabla T \tag{A2}$$

and

$$\mathbf{u} = 0. \tag{A3}$$

The problem with the baffles admits a no-motion state only when $k_s = k_f$ or $k_s/k_f \to 0$. In all other cases, we have an imperfect bifurcation. To accommodate any values of the diodes' thermal conductivity, we solve the problem numerically with finite elements. A sufficient number of elements are used to assure the grid independence of the computational results.

In the computations, we start with initial conditions that correspond to a no-motion state ($\mathbf{u}=0$) and a perturbed conductive temperature field $T=\lambda(0.5-z)$. We assume that $\rho_s=\rho_f$ and $C_{ps}=C_{pf}$, and we consider the cases $\zeta=k_s/k_f=0.1$, 1, and 10. We repeat the calculations for various values of the Rayleigh numbers. In each case, we computed the steady state kinetic energy $\int \mathbf{u}\cdot\mathbf{u}dA$ as a function of the Rayleigh number. Figure 13 depicts the kinetic energy $\int \mathbf{u}\cdot\mathbf{u}dA$ as a function of the normalized Rayleigh number when $a=H/35$, $P=51H/490$, $h=2H/35$, $\lambda=0.9$, and $\zeta=0.1$, 1, and 10. The Rayleigh number is scaled with the critical Rayleigh number of 2065 for a square box in the absence of baffles. When the bifurcation is imperfect, the critical Rayleigh number is defined as the Rayleigh number value at which a sharp change of slope occurs in the curve of the kinetic energy versus the Rayleigh number.

Witness that the numerical simulations indicate that the presence of baffles increases significantly the critical Rayleigh number for the onset of convection.

[1] S. Chandrasekhar, *Hydrodynamic and Hydromagnetic Stability* (Oxford, New York, 1969).
[2] S. H. Davis, "Stability of time-periodic flows," Annu. Rev. Fluid Mech. **8**, 57 (1976).
[3] R. J. Donnelly, "Externally modulated hydrodynamic systems," in *Nonlinear Evolution of Spatio Temporal Structures in Dissipative Continuous Systems* (Plenum, New York, 1990), p. 31.
[4] M. N. Roppo, S. H. Davis, and S. Rosenblat, "Benard convection with time periodic heating," Phys. Fluids **27**, 796 (1984).
[5] R. E. Kelly, "Stabilization of Rayleigh-Benard convection by means of a slow nonplanar oscillatory flow," Phys. Fluids A **4**, 647 (1992).
[6] R. E. Kelly and H. C. Hu, "The onset of Rayleigh-Benard convection in a nonplanar oscillatory flow," J. Fluid Mech. **249**, 373 (1993).
[7] R. E. Kelly and H. C. Hu, "The effect of finite amplitude non-planar flow oscillations upon the onset of Rayleigh-Benard convection," Proc. 10th International Heat Transfer Conference, 1994, Vol. 7, p. 79.
[8] J. Singer, Y-Z. Wang, and H. H. Bau, "Controlling a Chaotic System," Phys. Rev. Lett. **66**, 1123 (1991).
[9] J. Singer and H. H. Bau, "Active control of convection," Phys. Fluids A **3**, 2859 (1991).
[10] Y-Z. Wang, J. Singer, and H. H. Bau, "Controlling chaos in a thermal convection loop," J. Fluid Mech. **237**, 479 (1992).
[11] P. K. Yuen and H. H. Bau, "Rendering subcritical Hopf bifurcation supercritical," J. Fluid Mech. **317**, 91 (1996).
[12] P. K. Yuen, "Dynamics and control of flow in a thermal convection loop," Ph.D.dissertation, University of Pennsylvania, 1997.
[13] J. Tang and H. H. Bau, "Stabilization of the no-motion state in Rayleigh-Bénard convection through the use of feedback control," Phys. Rev. Lett. **70**, 1795 (1993).
[14] J. Tang and H. H. Bau, "Feedback control stabilization of the no-motion state of a fluid confined in a horizontal porous layer heated from below," J. Fluid Mech. **257**, 485 (1993).
[15] J. Tang and H. H. Bau, "Stabilization of the no-motion state in the Rayleigh-Bénard problem," Proc. R. Soc. London, Ser. A **447**, 587 (1994).
[16] J. Tang and H. H. Bau, "Stabilization of the no-motion state of a horizontal fluid layer heated from below with Joule heating," J. Heat Transfer **117**, 329 (1995).
[17] J. Tang and H. H. Bau, "Experiments on the stabilization of the no-motion state of a fluid layer heated from below and cooled from above," J. Fluid Mech. **363**, 153 (1998).
[18] J. Tang and H. H. Bau, "Numerical investigation of the stabilization of the no-motion state of a fluid layer heated from below and cooled from above," Phys. Fluids **10**, 1597 (1998).
[19] L. E. Howle, "Linear stability analysis of controlled Rayleigh-Bénard convection using shadowgraphic measurement," Phys. Fluids **9**, 3111 (1997).
[20] L. E. Howle, "Control of Rayleigh-Bénard convection in a small aspect ratio container," Int. J. Numer. Methods Fluids **40**, 817 (1997).
[21] L. E. Howle, "Active control of Rayleigh-Bénard convection," Phys. Fluids **9**, 1861 (1997).
[22] L. E. Howle, "The effect of boundary properties on controlled Rayleigh-Bénard convection," J. Fluid Mech. **411**, 39 (2000).
[23] T. A. Shortis and P. Hall, "on the effect of feedback control on Benard convection," NASA Contractor Report 198280, ICASE Report No. 96-9 (1996).
[24] A. C. Or, L. Cortelezzi, and J. L. Speyer, "Robust feedback control of Rayleigh-Bénard convection," J. Fluid Mech. **437**, 175 (2001).
[25] A. C. Or and J. L. Speyer, "Active suppression of finite-amplitude Rayleigh-Bénard convection," J. Fluid Mech. **483**, 111 (2003).
[26] A. C. Or and J. L. Speyer, "Gain-scheduled controller for the suppression of convection at high Rayleigh number," Phys. Rev. E **71**, 046302 (2005).
[27] P. K. Kundu and I. M. Cohen, *Fluid Mechanics* (Academic, San Diego, 2002).
[28] Femlab is a product of COMSOL Inc. Sweden (http://www.femlab.com).